


FBXO2/SCF ubiquitin ligase complex directs xenophagy through recognizing bacterial surface glycan

Akihiro Yamada , Miyako Hikichi, Takashi Nozawa  & Ichiro Nakagawa* 

Abstract

Xenophagy, also known as antibacterial selective autophagy, degrades invading bacterial pathogens such as group A *Streptococcus* (GAS) to defend cells. Although invading bacteria are known to be marked with ubiquitin and selectively targeted by xenophagy, how ubiquitin ligases recognize invading bacteria is poorly understood. Here, we show that FBXO2, a glycoprotein-specific receptor for substrate in the SKP1/CUL1/F-box protein (SCF) ubiquitin ligase complex, mediates recognition of GlcNAc side chains of the GAS surface carbohydrate structure and promotes ubiquitin-mediated xenophagy against GAS. FBXO2 targets cytosolic GAS through its sugar-binding motif and GlcNAc expression on the GAS surface. FBXO2 knockout resulted in decreased ubiquitin accumulation on intracellular GAS and xenophagic degradation of bacteria. Furthermore, SCF components such as SKP1, CUL1, and ROC1 are required for ubiquitin-mediated xenophagy against GAS. Thus, SCF^{FBXO2} recognizes GlcNAc residues of GAS surface carbohydrates and functions in ubiquitination during xenophagy.

Keywords bacterial surface glycan; group A *Streptococcus*; ubiquitination; xenophagy

Subject Categories Autophagy & Cell Death; Microbiology, Virology & Host Pathogen Interaction; Post-translational Modifications & Proteolysis

DOI 10.15252/embr.202152584 | Received 1 February 2021 | Revised 26 July 2021 | Accepted 20 August 2021 | Published online 13 September 2021

EMBO Reports (2021) 22: e52584

Introduction

Autophagy is a membrane trafficking process in which double-membrane spherical structures known as autophagosomes deliver cytosolic contents to lysosomes for degradation. Autophagy not only degrades its components but also selectively targets invading microbes and plays a key role in innate immune defense. Autophagy against microbes is named xenophagy and has been reported to degrade various intracellular bacterial pathogens such as *Mycobacterium tuberculosis*, *Salmonella enterica* serovar Typhimurium, and group A *Streptococcus* (GAS) (Levine & Deretic, 2007; Campoy &

Colombo, 2009). Intracellular bacteria are marked with ubiquitin and ubiquitin-binding autophagy receptors such as p62 and NDP52 and are recruited for linking to LC3 on autophagosomes (Boyle & Randow, 2013). Ubiquitin is also involved in recruiting ATG16L1 for xenophagy (Fujita *et al.*, 2013). Although ubiquitin ligases such as LRSAM1, Parkin, Smurf1, Nedd4-1, and RNF213 have been identified as crucial factors in xenophagy against various bacterial pathogens (Huett *et al.*, 2012; Manzanillo *et al.*, 2013; Franco *et al.*, 2017; Ogawa *et al.*, 2018; Otten *et al.*, 2021), how these ligases selectively recognize invading pathogens is poorly understood.

Group A *Streptococcus*, also known as *Streptococcus pyogenes*, is a group of gram-positive bacteria that cause a variety of illnesses, including pharyngitis, impetigo, and severe systemic infections such as necrotizing fasciitis and streptococcal toxic shock syndrome (Cole *et al.*, 2011). GAS invades non-phagocytic human cells via endocytosis and escapes from endosomes into the cytosol through the activity of streptolysin O (SLO), a pore-forming toxin secreted by GAS. GAS exposed to the cytoplasm is selectively targeted by xenophagy (Nakagawa *et al.*, 2004). Some GAS strains avoid xenophagic degradation by secreting toxins (Barnett *et al.*, 2013; O'Seaghdha & Wessels, 2013; Toh *et al.*, 2020). We previously reported that GAS invasion through SLO triggers the recruitment of ubiquitin-binding autophagy receptors to ubiquitin-marked GAS through TBC1D9 and RAB35 (Minowa-Nozawa *et al.*, 2017; Nozawa *et al.*, 2020), suggesting that ubiquitination is essential for xenophagy against GAS infection. However, the substrate(s) and ligase(s) responsible for ubiquitin-coating GAS have not been identified.

In addition to ubiquitin-mediated recognition, glycan binding proteins such as galectin-3 and galectin-8 have been reported to direct xenophagy by binding host glycans exposed on damaged endosomes and lysosomes. Galectin-8, a cytosolic β -galactoside-binding lectin, activates xenophagy by recruiting the autophagy receptor NDP52 during *Salmonella* Typhimurium infection (Thurston *et al.*, 2012). Galectin-3 recruits TRIM16, a RING-type ubiquitin ligase, to add K63-linked ubiquitin to damaged endomembranes (Chauhan *et al.*, 2016). In addition, although not involved in xenophagy, the SCF^{FBXO27} ubiquitin ligase complex has been reported to ubiquitinate lysosomal glycoprotein exposed following membrane damage for lysophagy (Yoshida *et al.*, 2017). Therefore, recent advances have revealed that glycan recognition is important for

xenophagy and lysophagy. The recognized glycan substrate is thought to be a host membrane component. However, despite the abundance of glycans and glycoproteins on the bacteria surface, whether bacterial glycans are also recognized in xenophagy is unknown.

Group A carbohydrate (GAC) is a bacterial surface rhamnose polysaccharide that constitutes half of the cell wall of GAS, is essential for bacterial growth, and contributes to infection ability (McCarty, 1952). The *N*-acetylglucosamine (GlcNAc) side chain, present in GAC, is a virulence factor (Henningham et al, 2018). Recent studies showed that mutants defective in GlcNAc side chain addition improve intracellular viability by increasing the sensitivity to neutrophils and serum killing, attenuating virulence, and suppressing host immune responses (van Sorge et al, 2014). However, it is unclear how the GAS surface carbohydrate structure and its GlcNAc side chains contribute to the intracellular dynamics of GAS in host cells.

In this study, we investigated the involvement of GlcNAc residues of GAS surface carbohydrate and FBXO2, a glycoprotein-specific F-box protein, in xenophagy. Our findings reveal that the bacterial sugar chain is among the markers of xenophagy recognition, providing insight into the pathway linking bacterial surface components and ubiquitin ligase in xenophagy.

Results

GAC side chain GlcNAc is involved in xenophagy of GAS

Although recent studies showed that ubiquitin-binding autophagy receptors are required for the xenophagy of GAS (Ito et al, 2013; Minowa-Nozawa et al, 2017; Lin et al, 2019), whether ubiquitin itself directly mediates xenophagy is not clear. To investigate the necessity of ubiquitination in xenophagy during GAS infection, we used the ubiquitin-activating enzyme (E1)-specific inhibitor PYR41, which blocks ubiquitination in cells (Yang et al, 2007). Human epithelial cells (HeLa cells) were treated with PYR41 and infected with GAS. The recruitment of galectin-3 was not affected by PYR41 treatment (Fig EV1A and B), suggesting that PYR41 does not inhibit GAS invasion into the host cytosol. In control (non-PYR41-treated) cells, intracellular GAS was coated with ubiquitin, whereas ubiquitin-positive GAS was rarely observed in PYR41-treated cells (Fig EV1A and B). Additionally, PYR41 treatment significantly decreased LC3-positive GAS (Fig EV1A and B). Because LC3 recruitment to bacteria is a hallmark of xenophagy induction (Xu et al, 2019), these results suggest that ubiquitination is required for the xenophagy of GAS.

Next, to investigate whether ubiquitination is required for xenophagic degradation of GAS, we examined the intracellular survival of GAS in PYR41-treated cells. Although the invasion efficiency of GAS was unchanged (Fig EV1C), the survival of bacteria at 6 h after infection was significantly increased upon PYR41 treatment (Fig EV1D). Taken together, these results suggest that ubiquitination is required for xenophagy against GAS.

We next observed the localization of galectin-3 and ubiquitin in GAS-infected cells and found that some ubiquitin-coated GAS was galectin-3-negative (Fig EV1E). Because galectin-3 targets damaged endosomal membranes (Paz et al, 2010), structures other than

damaged endosomal membranes may be targeted by the ubiquitination system during GAS infection.

The GAS surface harbors the GAC comprised of a polyrhamnose backbone with GlcNAc side chains. Twelve GAC genes (*gacA-gacL*) are involved in GAC biosynthesis and transport (Rush et al, 2017). The first three genes, *gacA-gacC*, are responsible for polyrhamnose backbone biosynthesis and are essential for bacterial viability, and *gacI-gacK* are required for the addition of GlcNAc side chains to the polyrhamnose backbone (Fig 1A). To examine the involvement of GAC components in xenophagy, we constructed GAC deletion mutants of GAS. We obtained six *gac* mutants of Δ *gacG-gacL*, but not of Δ *gacA-gacF*, which are thought to be critical for core rhamnose backbone construction. To determine whether these mutants were deficient in GlcNAc expression on the GAS surface, we treated GAS mutants with succinylated wheat germ agglutinin (sWGA), a lectin that specifically binds GlcNAc, and measured the fluorescence intensity of sWGA attached to each strain (Nagata & Burger, 1974). As expected, binding of sWGA to Δ *gacI* was not observed, and the deletion of *gacJ* and *gacK* significantly decreased sWGA binding to GAS (Fig 1B). These data are consistent with the results of a previous study (van Sorge et al, 2014). We then examined whether targeting of these GAC mutants by xenophagy was reduced. We found that LC3-positive GAS was significantly reduced in Δ *gacI*-, Δ *gacJ*-, and Δ *gacK*-infected cells than in wild-type GAS-infected cells (Fig 1C and D). In addition, although Δ *gacL* harbored GlcNAc on the cell surface, targeting LC3 to Δ *gacL* significantly decreased (Fig 1B and D). As *GacL* is required to transfer GlcNAc from GlcNAc-phosphate-undecaprenol to polyrhamnose, GlcNAc bound to the rhamnose backbone may be involved in xenophagy induction.

GlcNAc residues are involved in recognition by the host ubiquitination system

To validate the involvement of GlcNAc of GAS in xenophagy, we complemented *gacI* to Δ *gacI* because deletion of *gacI* most profoundly decreased GlcNAc expression on GAS. The recovery of GlcNAc expression was confirmed by the sWGA binding assay (Fig 2A). To confirm that *gacI* was involved in xenophagy induction, we examined LC3 lipidation levels during infection. The levels of the lipidated form of LC3 (LC3-II) during Δ *gacI* infection were significantly lower than those during GAS wild-type and Δ *gacI::gacI* infection (Fig 2B and C), suggesting that GlcNAc is involved in xenophagy induction during GAS infection. We next investigated which step upstream of LC3 recruitment (endocytosis, internalization of GAS, cytosolic escape via SLO, or recognition of GAS by the ubiquitination machinery) was affected by *gacI* deletion. The invasion efficiency of Δ *gacI* GAS cells was comparable to that of wild-type GAS (Fig EV2A), and recruitment of galectin-3 was unchanged (Fig EV2B and C), demonstrating that GlcNAc was not associated with bacterial invasion into the host cytosol. We found that deletion of *gacI* resulted in decreased ubiquitin-coated GAS (Fig 2D and E). To validate whether GlcNAc residues are involved in ubiquitination during GAS infection, we isolated bacteria from infected cells through affinity purification using anti-lipoteichoic acid antibodies. Similar numbers of wild-type and Δ *gacI* GAS were isolated from host cells at 4 h after infection (Fig EV2D). We then detected

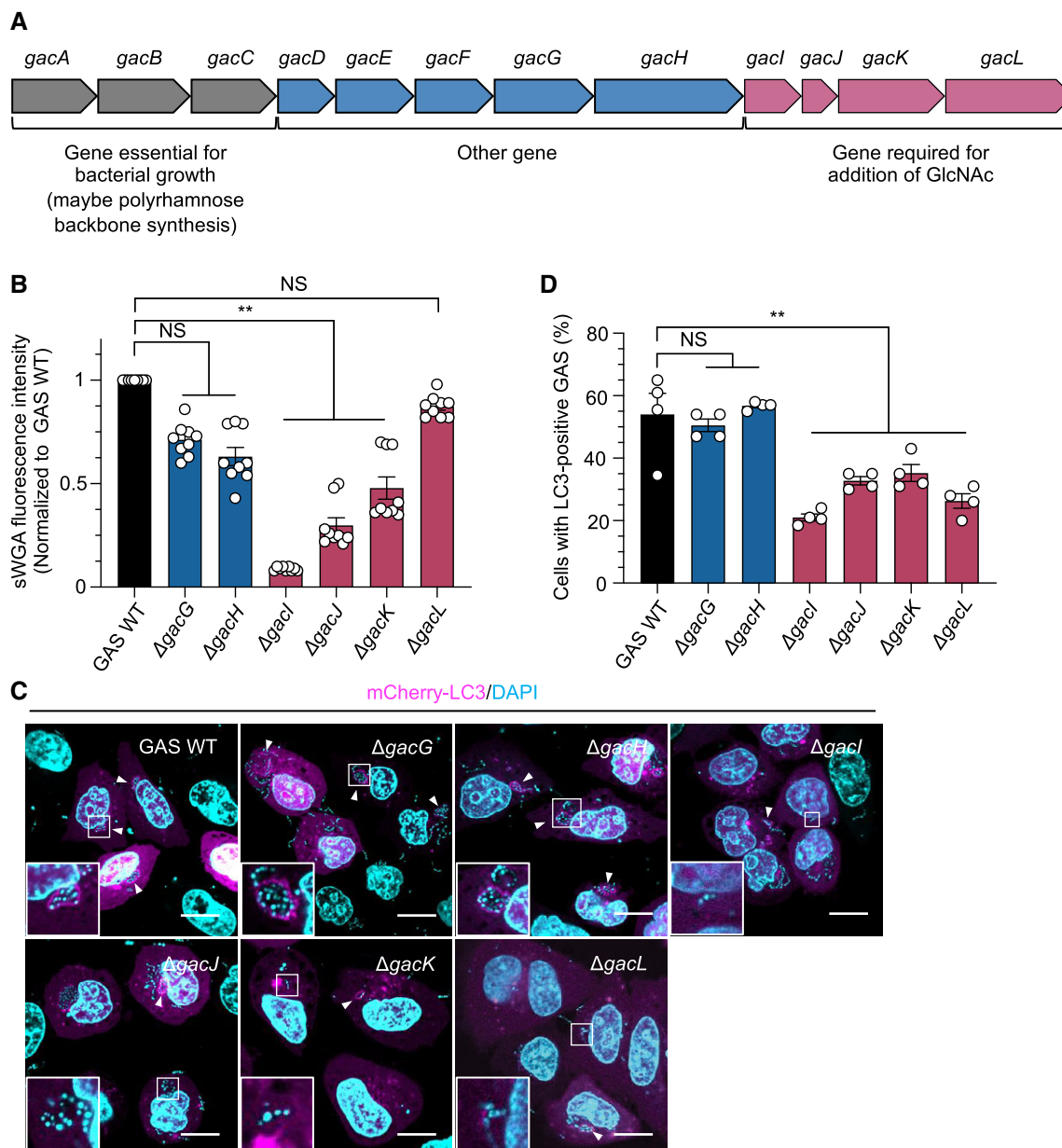


Figure 1. Screening of *gac* deletion mutant.

A Schematic representation of the group A carbohydrate (GAC) gene cluster. Biogenesis of GAC is obtained with 12 *gac* operons. Genes from *gacA* to *gacC* are responsible for rhamnose backbone biogenesis, and those from *gacI* to *gacL* are involved in GlcNAc side chain addition.

B Expression levels of GlcNAc in wild-type (WT) GAS, $\Delta gacG$, *H*, *I*, *J*, *K*, and *L* were measured as the sWGA fluorescence intensity (normalized to WT GAS).

C, D HeLa cells expressing mCherry-LC3 (magenta) were infected with WT GAS and the indicated *gac* deletion mutant for 2 h at an MOI of 100 and then stained with DAPI (cyan); scale bar, 10 μ m. (C) Representative confocal images are shown at 2 h post-infection, and (D) percentages of GcAV-positive cells were quantified.

Data information: Data represent the mean \pm SEM of (B) nine and (D) four independent experiments. Asterisks indicate significant differences (** $P > 0.01$) as determined by Student's *t*-test.

conjugated ubiquitin by immunoblotting and found that isolated wild-type GAS carried multiple ubiquitinated molecules with 100–200 and 17 kDa (Fig 2F). In contrast, the size of the bands from $\Delta gacI$ GAS was 140–200 kDa (Fig 2F), indicating that GlcNAc residues on the GAS surface are involved in ubiquitination of bacteria in infected cells.

To confirm the involvement of GlcNAc residues in ubiquitin-mediated recognition in xenophagy, we pre-treated GAS with sWGA to mask GlcNAc residues on the bacterial surface and infected cells with sWGA-coated GAS. Pre-treatment of GAS with sWGA did not inhibit the recruitment of galectin-3 to GAS (Fig EV2E and F) but significantly decreased ubiquitin-positive GAS in wild-type and

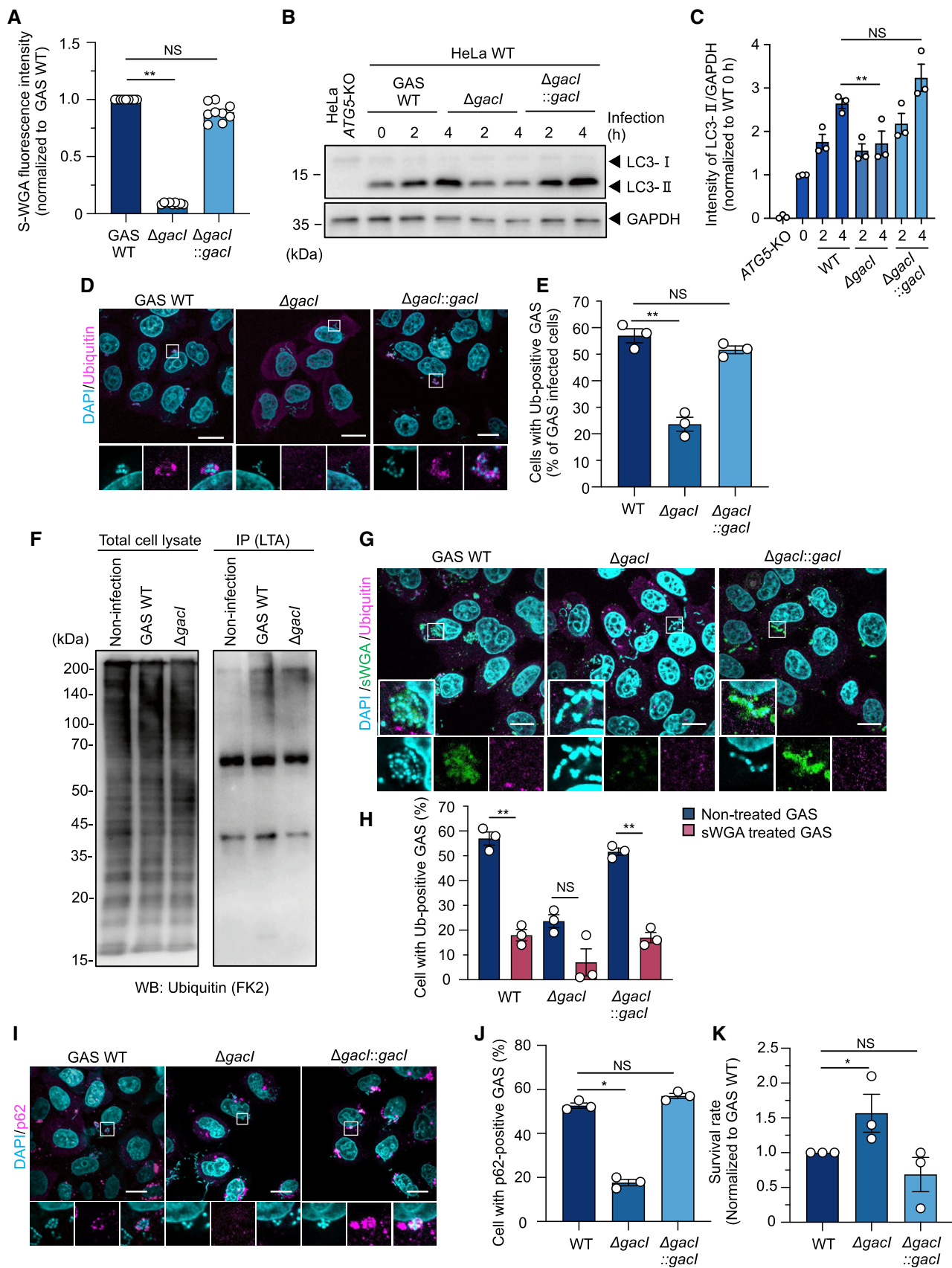


Figure 2.

Figure 2. GlcNAc affects ubiquitination of GAS.

- A Expression levels of GlcNAc in WT GAS, Δ *gacl*, and Δ *gacl::gacl* were measured as the sWGA fluorescence intensity (normalized to WT GAS).
 B, C Accumulation of LC3-II. (B) Representative Western blot of LC3-II during non-infection (NI), WT GAS, Δ *gacl*, and Δ *gacl::gacl*. (C) LC3-II intensity normalized to NI.
 D, E Recruitment of ubiquitin in GAS-infected cells. HeLa cells were infected with WT GAS, Δ *gacl*, and Δ *gacl::gacl* for 4 h, fixed, and immunostained for ubiquitin (FK2: magenta). Cellular and bacterial DNAs were stained with DAPI (cyan). (D) Representative confocal images and (E) percentage of cells with ubiquitin-positive GAS. Scale bar, 10 μ m.
 F Immunoblot of the indicated GAS isolated from host cells. Lysate of GAS-infected HeLa cells was precipitated with anti-lipoteichoic acid antibody to isolate GAS, and the immunoprecipitates were analyzed by immunoblotting.
 G, H Localization of ubiquitin in sWGA-treated GAS. HeLa WT was infected with the indicated GAS strains masked with sWGA for 4 h, fixed, and immunostained for ubiquitin (magenta). (G) Representative confocal images and (H) percentages of cell with ubiquitin-positive GAS. Scale bar, 10 μ m.
 I, J Recruitment of p62 to *gacl* mutants. HeLa cells were infected with WT GAS, Δ *gacl*, and Δ *gacl::gacl* for 4 h, fixed, and immunostained for p62 (magenta). Cellular and bacterial DNAs were stained with DAPI (cyan). (I) Representative confocal images and (J) percentage of cells with p62-positive GAS. Scale bar, 10 μ m.
 K Bacterial viability rates of GAS mutants in cells (CFU recovered at 6 h post-infection/CFU at 2 h post-infection).

Data information: Data are shown as the mean \pm SEM of (A) nine and (C, E, H, J, and K) three independent experiments. Asterisks indicate significant differences (* $P > 0.05$, ** $P > 0.01$) as determined by Student's *t*-test.

Source data are available online for this figure.

Δ *gacl::gacl*-infected cells (Fig 2G and H). In contrast, no significant reduction in ubiquitin-positive GAS was observed after sWGA treatment in Δ *gacl*-infected cells (Fig 2G and H). Taken together, these results demonstrate that GlcNAc residues are involved in bacterial recognition by the ubiquitination system for xenophagy during GAS infection.

As ubiquitin-coated GAS is recognized by ubiquitin-binding autophagy receptors such as p62, we next examined the recruitment of p62 to invading GAS. Deletion of *gacl* abolished the recruitment of p62, whereas complementation of *gacl* restored the p62 recruitment to GAS (Fig 2I and J). Because targeting of Δ *gacl* GAS by ubiquitin, p62, and LC3 was decreased, we next examined whether this mutant avoided xenophagic degradation. The survival rate of Δ *gacl* GAS was significantly higher than that of the wild-type and Δ *gacl::gacl* GAS strains (Fig 2K). Therefore, GlcNAc is involved in recognition by host ubiquitin-mediated xenophagy.

GlcNAc residues induce K48- and K63-ubiquitin coating during GAS infection

K48-, K63-, and M1-linked polyubiquitination is reportedly crucial for xenophagy (Ito *et al*, 2013; Noad *et al*, 2017; Ogawa *et al*, 2018). K48-ubiquitin signals coated each bacterium, whereas K63-ubiquitin signals localized around aggregated bacteria (Fig EV3A). In contrast, minimal M1-linked linear ubiquitin signals were detected around GAS (Fig EV3A). This observation is consistent with the localization of ubiquitin during *Streptococcus pneumoniae* (Ogawa *et al*, 2018). To determine the types of polyubiquitin chains induced via GAS surface GlcNAc residues, we observed chain-specific ubiquitin signals on *gacl* mutants. Confocal microscopic images revealed that the recruitment of both K48 ubiquitin and K63 ubiquitin during Δ *gacl* infection was reduced compared with that during wild-type and Δ *gacl::gacl* infection (Fig EV3B and C). Therefore, GlcNAc on the GAS surface is involved in inducing both K48 ubiquitination and K63 ubiquitination during xenophagy of GAS.

GAS is targeted by FBXO2 through GlcNAc residues

Because GlcNAc residues on the GAS surface carbohydrate were suggested to be involved in ubiquitin-mediated recognition during GAS infection, we focused on glycoprotein-specific F-box proteins (FBXO2, FBXO6, and FBXO27), which are components of the SCF

ubiquitin ligase complex (Yoshida *et al*, 2002). We determined the subcellular localization of EmGFP-tagged FBXO2, FBXO6, and FBXO27 during GAS infection. EmGFP-FBXO2 and EmGRP-FBXO6 were recruited to intracellular GAS, whereas EmGFP-FBXO27 was not (Fig 3A). More than 50 and 30% of infected cells exhibited FBXO2- and FBXO6-positive GAS, respectively (Fig 3B). Confocal microscopy images show that FBXO2 and FBXO6 were co-localized with LC3, and some GAS-associated FBXO2 signals were LC3-negative (Fig 3C, arrowhead). Furthermore, signal-intensity plots of FBXO2 and LC3 revealed that the signal peaks of FBXO2 were inside the LC3-positive circles (Fig 3C), suggesting that FBXO2 targets bacteria rather than LC3 vacuoles. We also examined the kinetics of the recruitment of FBXO2 and LC3 to GAS and found that FBXO2 was recruited to GAS more frequently than LC3 at 2 and 4 h after infection (Fig 3D). To determine whether FBXO2 targeted cytosolic GAS, we observed the localization of FBXO2 during WT or Δ *slo* GAS infection. As shown in Fig EV4A–D, galectin-3, LC3, and FBXO2 were not recruited to Δ *slo* GAS, suggesting that FBXO2 translocation occurred proximal to invading bacteria upon cytosolic escape through SLO during GAS infection. Because LC3 recruitment to GAS was ubiquitination-dependent and decreased after infection with a GlcNAc deletion mutant, we examined the recruitment of FBXO2 to Δ *gacl* GAS. Recruitment of FBXO2 to GAS decreased after *gacl* deletion (Fig 3E and F), suggesting that GlcNAc is involved in targeting FBXO2 to GAS. Taken together, these results suggest that invading GAS is targeted by FBXO2 through GAS surface GlcNAc residues.

FBXO2 targets intracellular GAS through sugar-binding motifs

FBXO2 consists of four distinct domains: the PEST domain (residues 1–54), F-box domain (FBD; residues 55–95), linker domain (residues 96–124), and sugar-binding domain (SBD; residues 125–297). FBD binds to SKP1 and SBD binds to the innermost chitobiose in high-mannose *N*-glycans, but mutations Y279 and W280 in SBD prevent this binding (Mizushima *et al*, 2004). To investigate the translocation mechanism of FBXO2 to GAS in more detail, we constructed a series of deletion and substitution mutants of FBXO2 (Fig 4A). FBXO2 Δ FBD was localized to GAS, whereas the FBXO2 Y279A, W280A, and Y279A/W280A mutants showed cytosol and nuclear localization and were not recruited to GAS (Fig 4B and C), demonstrating that the sugar-binding motif is critical for targeting of FBXO2 to invading GAS.

To further examine whether FBXO2 directly binds to the GAS surface, we incubated GAS cells with EmGFP-FBXO2 or EmGFP-FBXO2^{Y279A/W280A} *in vitro*. Interestingly, EmGFP-FBXO2 was precipitated with wild-type GAS in a sugar-binding motif-dependent manner *in vitro* but not with Δ gacl GAS (Fig 4D). These results indicate that FBXO2 directly binds to GAS cells through the GlcNAc side chain of GAS and sugar-binding properties. Although we examined the involvement of SCF components in FBXO2 localization, SKP1,

CUL1, and ROC1 were not required to recruit FBXO2 to GAS (Fig 4E and F).

FBXO2 is involved in xenophagy

In human cell lines, FBXO2 expression was detected by Western blotting in epithelial cell lines (HeLa and A549 cells) but not in endothelial cells (HUVEC and HMEC-1; Fig 5A). To understand the

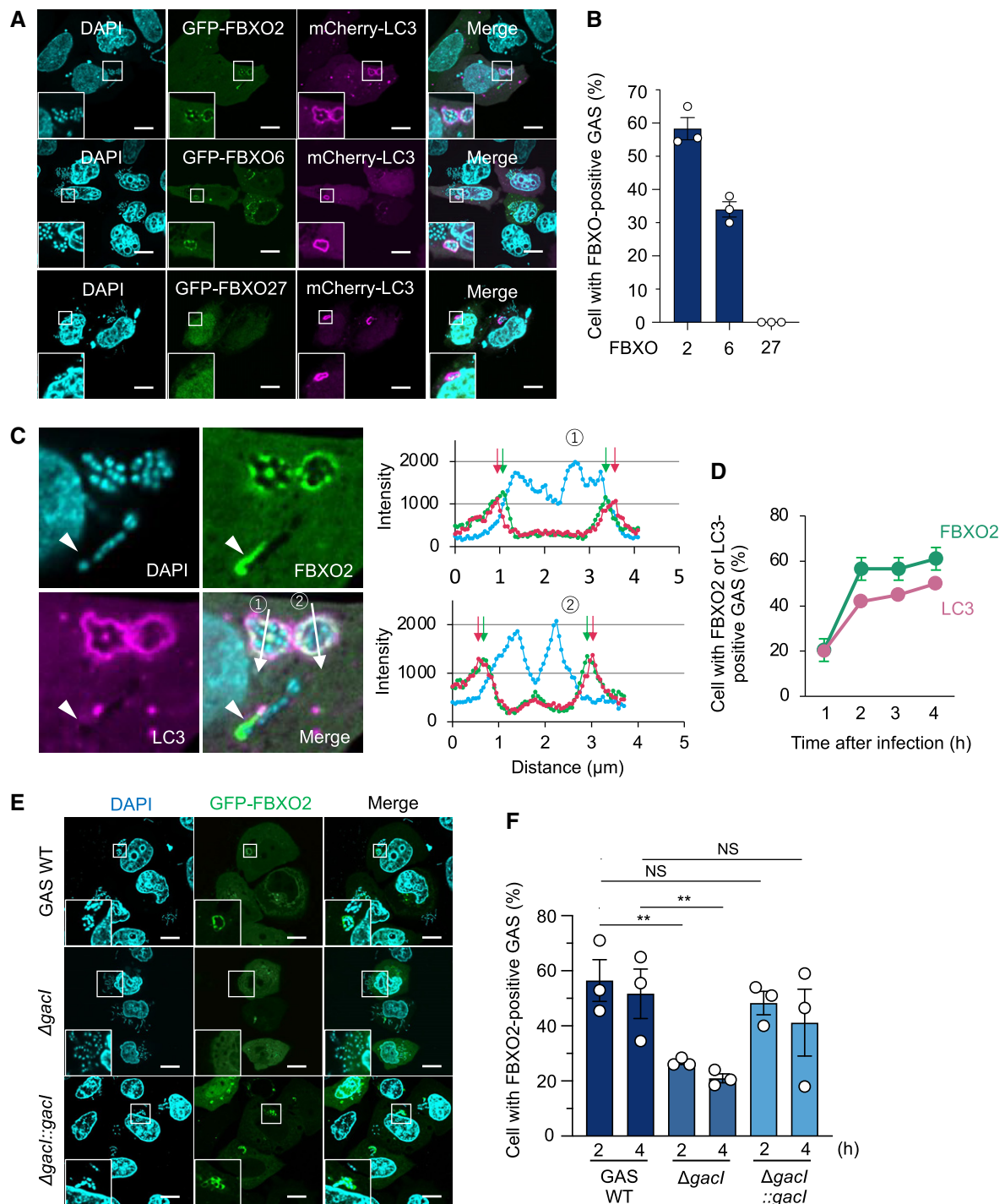


Figure 3.

Figure 3. FBXO2 targets GAS and is involved in xenophagy.

- A, B Co-localization of GFP-FBXO2 and mCherry-LC3 in GAS-infected cells. HeLa cells transfected with the indicated EmGFP-FBXO2 (green) and mCherry-LC3 (magenta) were infected with WT GAS for 2 h; scale bar, 10 μ m. Representative confocal images (A) and (B) percentages of FBXO2-positive cells.
- C Enlarged image of GAS-associated FBXO2 of (A). Graphs show the signal intensities of EmGFP-FBXO2 and mCherry-LC3 measured along the arrows in the merged image. Green and red arrows indicate the signal peaks observed in EmGFP-FBXO2 and mCherry-LC3, respectively. White arrow indicates bacteria that are targeted by FBXO2 but not by LC3. Scale bar, 10 μ m.
- D Time course of FBXO2 and LC3 recruitment during GAS infection.
- E, F Localization of EmGFP-FBXO2 in GAS-infected cells. HeLa cells transfected with GFP-FBXO2 (green) were infected with the indicated GAS strains for 2 or 4 h at an MOI of 100; scale bar, 10 μ m. Representative confocal images at 4 h of WT GAS, Δ *gacl*, and Δ *gacl::gacl* (E) and (F) percentages of FBXO2-positive cells.
- Data information: Data are shown as the mean \pm SEM of (B–D, F; $n > 200$ cells per condition) three independent experiments. Asterisks indicate significant differences (** $P > 0.01$) as determined by Student's *t*-test.

role of FBXO2 in xenophagy against GAS, we constructed *FBXO2*-knockout (KO) HeLa cells using CRISPR/Cas9 genome editing (Fig EV4E). *FBXO2*-KO did not change bacterial invasion efficiency in host cells; however, GAS survival at 6 h after infection was significantly increased in *FBXO2*-KO cells compared with WT cells (Fig 5B and C), suggesting that FBXO2 is involved in the elimination of intracellular bacteria. We next observed intracellular GAS and found that knockout of *FBXO2* did not inhibit GAS invasion into the host cytosol (Fig 5D) but reduced ubiquitin-, p62-, and LC3-positive GAS (Fig 5E–J). To confirm these results, we examined the conversion of LC3-I to LC3-II to evaluate xenophagy induction. LC3-II levels increased upon GAS infection in WT cells, whereas LC3-II accumulation was not observed from 2 to 4 h after infection in *FBXO2*-KO cells (Fig 5K and L). Therefore, FBXO2 may be involved in ubiquitination against GAS infection to induce xenophagy.

Because FBXO2 was recruited to GlcNAc-harboring GAS through a sugar-binding motif (Fig 4B and C), we investigated whether recruitment of FBXO2 to GAS was functionally required for ubiquitination and xenophagy. We expressed WT FBXO2 or FBXO2^{Y289A/W290A} in *FBXO2*-KO cells and observed ubiquitin and LC3 levels during GAS infection. Both ubiquitin- and LC3-positive GAS were recovered by WT FBXO2 expression, but FBXO2^{Y289A/W290A} did not increase ubiquitin-coated or LC3-positive GAS in *FBXO2*-KO cells (Figs 5M and N, and EV4F). These results suggest that sugar-binding properties are required for FBXO2-mediated ubiquitination and LC3 recruitment during GAS infection.

To examine whether FBXO6 also functions redundantly or cooperatively with FBXO2, we knocked down the expression of FBXO2 and FBXO6 (Fig EV5A). Ubiquitin coating the bacteria was reduced in *FBXO6*-knockdown cells, although not to the same extent as in *FBXO2*-knockdown cells (Fig EV5B). However, knockdown of FBXO6 did not significantly decrease LC3-positive GAS, and double knockdown of FBXO2 and FBXO6 did not further enhance the effect

of FBXO2 knockdown (Fig EV5C). Thus, taken together, FBXO6 appears to be involved in ubiquitination during GAS infection, although FBXO2 plays a prominent role in this process.

FBXO2-containing SCF complex is involved in xenophagy

To examine whether FBXO2 functions as a component of the SCF ubiquitin ligase complex, we knocked down SKP1, CUL1, and ROC1 expression using siRNA in HeLa cells (Fig EV5D). Recruitment of ubiquitin and LC3 to GAS was significantly decreased after knockdown of SKP1, CUL1, and ROC1 (Fig 6A–C). To confirm the involvement of FBXO2-mediated SCF components in ubiquitination and xenophagy during GAS infection, we treated the cells with an NEDD-8 inhibitor (MLN4924) and examined the number of ubiquitin- and LC3-positive bacteria. Treatment with MLN4924 significantly decreased ubiquitin- and LC3-positive GAS (Fig 6D and E). Therefore, the SCF complex is involved in ubiquitination and xenophagy against GAS infection.

Finally, to validate whether FBXO2 recruits SCF complex to invading GAS, we examined the interaction between FBXO2 and SCF components during infection. Co-immunoprecipitation revealed that SKP1, CUL1, and ROC1 interact with FBXO2 during GAS infection (Fig EV5E). We also isolated GAS from WT and *FBXO2*-KO cells and detected precipitated SCF components. As expected, intracellular GAS carried CUL1, SKP1, and ROC1 in an FBXO2-dependent manner (Fig 6F), indicating that FBXO2 recruits the SCF complex to intracellular GAS for ubiquitination.

Discussion

Ubiquitination is a critical step in xenophagy, but the underlying mechanism by which ubiquitin ligase selectively targets the substrate is poorly understood. Furthermore, ubiquitin ligases that

Figure 4. FBXO2 targets intracellular GAS through sugar-binding motifs.

- A Schematic representation of wild-type FBXO2 and domain deletion mutants of FBXO2. Numbers above the constructs represent the amino acid positions of FBXO2. PEST (residues 1–54) and F-box domains (residues 55–95), linker sequence (residues 96–124), and sugar-binding domain (residues 125–297) are indicated by P, FBD, linker, and SBD, respectively.
- B, C HeLa cells transfected with the indicated GFP-FBXO2 mutants (green) were infected with WT GAS for 4 h; scale bar, 10 μ m. Representative confocal images (B) and percentages of each FBXO2 mutants localized to GAS (C).
- D EmGFP intensities bound to GAS cells *in vitro*. GAS cells were incubated cell lysate expressing EmGFP, EmGFP-FBXO2, or EmGFP-FBXO2Y279A/W280A and precipitated EmGFP with GAS cells.
- E, F Recruitment of FBXO2 to intracellular GAS in SKP1/CUL1/ROC1 knockdown cells. HeLa cells transfected with GFP-FBXO2 (green) and the indicated siRNAs were infected with GAS, fixed at 4 h; scale bar, 10 μ m. Representative confocal images (E) and percentages of FBXO2 localized to GAS (F).
- Data information: Data are shown as the mean \pm SEM of three independent experiments. Asterisks indicate significant differences (** $P > 0.01$) as determined by Student's *t*-test.

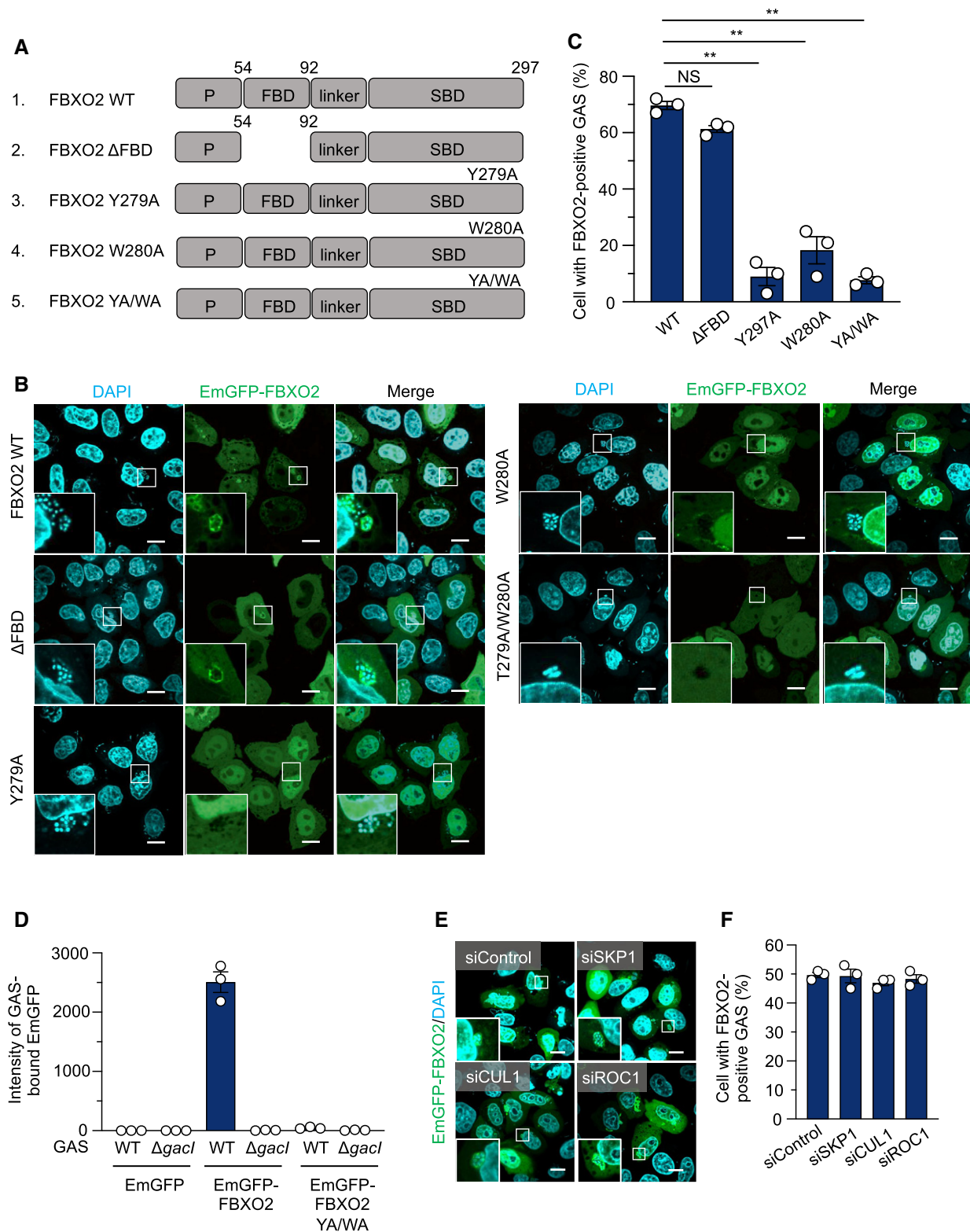


Figure 4.

directly recognize bacterial components have not been reported. In this study, we found that the bacterial surface glycan is one of the SCF ubiquitin ligase complex targets through the glycoprotein-specific receptor FBXO2 (Fig 6G).

Because glycan recognition is an important event in the xenophagy process, we used GAS GAC mutants to show that mutants defective in GlcNAc addition to the rhamnose backbone were recognized less effectively by xenophagy. Notably, despite Δ gacL

showing GlcNAc expression at a level comparable to WT GAS, recognition of this mutant by xenophagy was lower (Fig 1B–D). Because GacL is a GT-C glycosyltransferase that transfers GlcNAc

from GlcNAc-P-Und to polyrhamnose, the *AgacI* mutant binds to SWGA via GlcNAc exposed on the cell surface (Rush *et al*, 2017), and therefore, the GlcNAc-attached rhamnose backbone may be

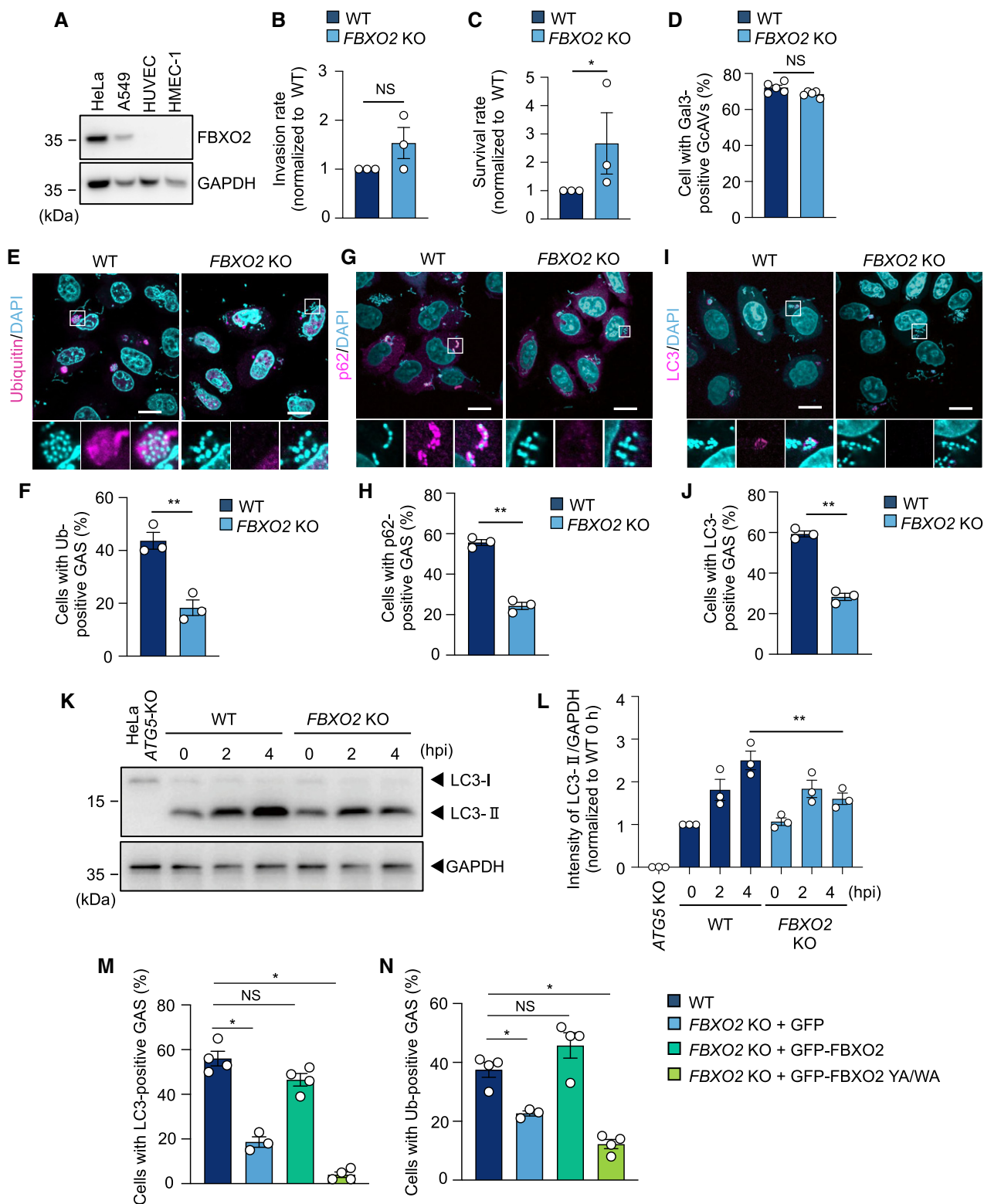


Figure 5.

Figure 5. FBXO2 is required for GAS xenophagy.

- A Western blotting of FBXO2 in human cell lines.
- B Bacterial invasion rates into host cells (CFU recovered at 2 h post-infection/CFU at 1 h post-infection) which were normalized to that in wild-type cells.
- C Intracellular bacterial survival rates (CFU recovered at 6 h post-infection/CFU at 2 h post-infection) which were normalized to that in wild-type cells.
- D HeLa WT or *FBXO2*-KO cells transfected with mCherry-Gal3 (magenta) were infected with WT GAS for 2 or 4 h, and percentages of Gal3-positive GAS-containing cells were quantified.
- E–J Localization of ubiquitin, LC3 and p62 in *FBXO2*-KO cells. HeLa WT or *FBXO2*-KO cells were infected with WT GAS for 4 h, fixed, and immunostained for ubiquitin (FK2: magenta) or LC3 (magenta) or p62 (magenta). Representative confocal images (E, G, and I) and percentages of cells with ubiquitin, LC3, or p62-positive GAS (F, H, and J).
- K, L Accumulation of LC3-II during GAS infection. (K) Representative Western blot of LC3 during infection. (L) LC3-II intensities normalized to non-infection condition of wild-type cells.
- M, N GlcNAc recognition of FBXO2 required for GAS xenophagy. Non-transfected HeLa WT cells and HeLa *FBXO2*-KO cells transfected GFP, GFP-FBXO2, and GFP-FBXO2 YW/AA were infected with GAS WT for 4 h, fixed, and immunostained for ubiquitin. Percentages of cells with LC3 (M) or ubiquitin (N)-positive GAS were quantified.

Data information: Data are shown as the mean \pm SEM of more than three independent experiments (B–D, F, H, J, and L–N), $n > 200$ cells per condition. Asterisks indicate significant differences (* $P > 0.05$, ** $P > 0.01$) as determined by Student's *t*-test.

Source data are available online for this figure.

necessary for recognition by FBXO2. This result is consistent with previous results showing that FBXO2 recognizes *N*-glycan rather than GlcNAc residues (Yoshida *et al*, 2002; Mizushima *et al*, 2004; Glenn *et al*, 2008). Importantly, although lower recruitment of FBXO2, ubiquitin, and LC3 occurred in the Δ *gacI* mutant than in the WT GAS, more than 20% of cells showed FBXO2-, ubiquitin-, and LC3-positive Δ *gacI* GAS (Figs 1D, 2E, and 3F). Thus, despite the fact that GlcNAc may not be completely absent from the GAS surface after deletion of *gacI*, the host GlcNAc residues may have been recognized by FBXO2 because GlcNAc is abundant in the cell membrane and FBXO2 binds to the lysosomal glycoprotein LAMP1 (Yoshida *et al*, 2017; Liu *et al*, 2020). Therefore, the FBXO2-mediated SCF ubiquitin ligase complex is involved in xenophagy during GAS infection through bacterial glycan recognition, but this ubiquitination machinery may also function in xenophagy against other pathogenic bacteria via host glycan sensing.

FBXO2, FBXO6, and FBXO27 are F-box-associated (FBA) families of F-box proteins, which contain a domain that mediates carbohydrate substrate binding. This domain is structurally homologous to the glycan binding domains of two other mammalian lectins, galectin (Mizushima *et al*, 2004) and PNGase F (Zhou *et al*, 2006). FBXO2, FBXO6, and FBXO27 bind high-mannose *N*-linked glycoproteins and function as ubiquitin ligase subunits for endoplasmic reticulum-associated degradation (Yoshida *et al*, 2002). Of these FBA family proteins, FBXO2 was most frequently recruited to intracellular GAS in HeLa cells (Fig 3A and B). We also investigated effects of FBXO6 knockdown in xenophagy of GAS, but the involvement of FBXO6 was modest compared with that of FBXO2. Although FBXO2 and FBXO6 show a homologous motif arrangement, it has been reported that FBXO6 binds glycoproteins less tightly compared with FBXO2 because the total length of SBD is slightly shorter in FBXO6 and the hydrophobic pocket required for binding to glycoproteins differs from that of FBXO2 (Glenn *et al*, 2008). Therefore, FBXO6 may be involved in an unrecognized target other than GAS. Previous reports showed that the FBXO27-containing SCF complex ubiquitinates lysosomal glycoprotein for lysophagy (Yoshida *et al*, 2017). However, FBXO27 expression is restricted to several tissues such as the brain, and its expression has not been detected in some human epithelial cells, including HeLa cells (Yoshida *et al*, 2017). FBXO2 is broadly expressed in systemic cells and is expressed at high

levels in the nervous system. Liu *et al* (2020) recently reported that FBXO2 mediates lysophagy in the central nervous system. Therefore, the FBA-containing SCF complex is suggested to mediate lysophagy and xenophagy in various tissues, and functional differences between FBA families may be related to FBA protein expression patterns. Here, we show that FBXO2 was expressed in human epithelial cells such as HeLa and A549 cells but not in endothelial cells (HUVECs and HMEC-1 cells). Because GAS can survive in endothelial cells because of the ubiquitination deficiency (Lu *et al*, 2017), reduced FBXO2 expression may be one reason for intrinsically defective xenophagy in endothelial cells.

We showed that bacterial surface glycan is recognized by the FBXO2-mediated SCF complex for ubiquitination in xenophagy during GAS infection because recognition of GlcNAc-deficient mutants or GlcNAc-masked GAS by FBXO2 and the autophagy machinery was reduced. However, which bacterial and/or host protein(s) are ubiquitinated remains unknown. FBXO2 is involved in clearing damaged lysosomes and binds to LAMP1, and SCF^{FBXO27} ubiquitinates VAMP3, VAMP7, LAMP1, LAMP2, GNS, PSAP, and TMEM192 during lysophagy (Yoshida *et al*, 2017). Although ubiquitin-binding bacterial proteins that promote xenophagy have been identified in *M. tuberculosis* (Chai *et al*, 2019), the bacterial proteins ubiquitinated by ubiquitin ligase during xenophagy have not been identified. Notably, Otten *et al* (2021) reported that non-proteinaceous lipopolysaccharide of *Salmonella* is ubiquitinated, which directs ubiquitin-dependent xenophagy.

Given that our results were showing that isolated bacteria from host cells carried multiple ubiquitinated products and that the band pattern differed among WT and Δ *gacI* mutants, the surface components of gram-positive GAS may be ubiquitinated. Further studies to explore ubiquitinated bacterial components would reveal the molecular mechanism of xenophagy. In addition, FBXO proteins play physiological roles other than as substrate receptors for the SCF complex, and identifying the functions of FBXO2 in xenophagy other than ubiquitination may lead to the detection of a novel xenophagy induction pathway.

In conclusion, we demonstrated the involvement of the GAC side chain and SCF ubiquitin ligase complex in bacterial infection. Observation of the interactions between GAS and host cells provides insights into the mechanisms by which host defense systems sense

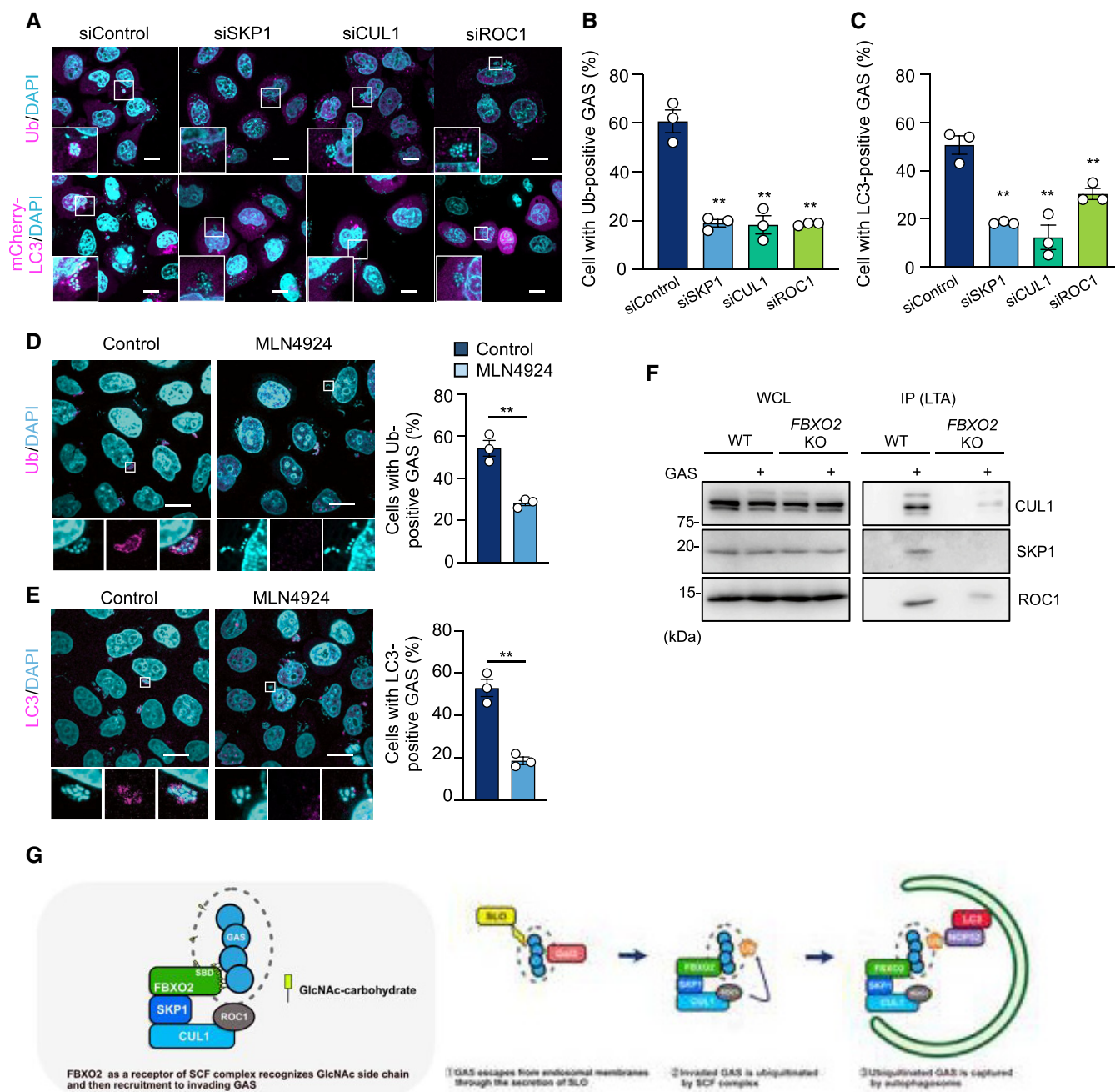


Figure 6. SCF complex is involved in ubiquitination and xenophagy against GAS infection.

A–C Recruitment of LC3 and ubiquitin to intracellular GAS in SKP1/CUL1/ROC1 knockdown cells. HeLa cells transfected with mCherry-LC3 (magenta) and the indicated siRNAs were infected with GAS for 4 h. Cells were immunostained for ubiquitin (FK2); scale bar, 10 μ m. Representative confocal images (A) and percentages of cells with ubiquitin (B) and LC3 (C)-positive GAS.

D, E Neddylated cullin inhibitor: MLN4924-treated HeLa cells were infected with WT GAS and fixed at 4 h. Cells were immunostained for ubiquitin (FK2; magenta) or LC3 (magenta); scale bar, 10 μ m. Representative images and quantification of cells with ubiquitin-positive GAS (D) and LC3-positive GAS (E).

F Lysates from HeLa cells infected with GAS were immunoprecipitated with an anti-lipoteichoic acid antibody and Protein G-Magnetic Beads. Immunoprecipitates were analyzed by immunoblotting.

G Proposed model for FBXO2-mediated recognition of bacterial glycan in xenophagy. GAS internalized via endocytosis enters the cytosol, and then, GAS escapes into the cytoplasm by SLO secretion. Escaped GAS is targeted by FBXO2 via recognition of GlcNAc and is ubiquitinated by the SCF complex. Finally, LC3 is recruited to ubiquitinated GAS for autophagy formation.

Data information: Data are shown as the mean \pm SEM of three independent experiments (B–E), $n > 200$ cells per condition. Asterisks indicate significant differences (** $P > 0.01$) as determined by Student's *t*-test.

Source data are available online for this figure.

GAS, which may improve the understanding of the pathogenesis of various diseases and lead to the identification of therapeutic targets.

Materials and Methods

Bacterial strains

GAS strain JRS4 (M6⁺, F1⁺) and gene deletion mutants were grown in Todd Hewitt broth (BD Diagnostic Systems, San Jose, CA, USA) supplemented with 0.2% yeast extract (THY), and tryptic-soy broth supplemented with 0.2% yeast extract for bacterial adhesion, internalization, and survival assays.

Generation of *gac* mutants and complemented strains

The 800-base pair (bp) upstream and downstream regions of the target gene were amplified from JRS4 genomic DNA using PrimeSTAR Max (TaKaRa, Shiga, Japan) and cloned into a thermosensitive suicide vector, pSET4s using the Gibson Assembly system (New England Biolabs, Ipswich, MA, USA). The recombinant plasmid was incorporated into GAS by electroporation, and transgenic GAS was spread onto THY agar media supplemented with spectinomycin, incubated for 2 days at 28°C, and transplanted into a 37°C chamber overnight to select single-crossover mutants. The single-crossover mutants were spread onto THY agar media and kept at 28°C for approximately 1 week with occasional transplantations. To generate complemented strains, the full-length deleted genes covering 800 bp upstream and downstream were amplified, cloned, and transfected into *gac* mutants using the same procedure described above.

Cell lines, culture conditions, and transfection

The HeLa and A549 cell lines were purchased from ATCC, and HUVECs and HMEC-1 cells were purchased from PromoCell (Heidelberg, Germany). HeLa, A549, and HMEC-1 cells were maintained in Dulbecco's modified Eagle's medium (Nacalai Tesque, Kyoto, Japan) supplemented with 10% fetal bovine serum (Gibco, Grand Island, NY, USA) and 50 µg/ml gentamicin (Nacalai Tesque) in a 5% CO₂ incubator at 37°C. HUVECs were maintained with endothelial cell growth medium 2 kit (PromoCell) supplemented with 10% fetal bovine serum and 50 µg/ml gentamicin. The transfection reagents used were polyethylenimine (Polysciences, Warrington, PA, USA) and Lipofectamine 3000 (Invitrogen, Carlsbad, CA, USA).

Binding of sWGA to bacteria

WT JRS4 and the JRS4 GAC deletion mutant strains grown in THY medium were washed three times with phosphate-buffered saline (PBS) and resuspended in PBS. GlcNAc-specific fluorescein-sWGA (FL-1021S; Vector Laboratories, Burlingame, CA, USA) was added to a final concentration of 10 µg/ml. After 30 min of incubation at room temperature with mixing, the bacterial cells were centrifuged, washed twice, and resuspended in PBS. Bound fluorescein-sWGA was quantified in a multi-label plate reader Wallac 1420 ARVOsx (PerkinElmer, Waltham, MA, USA) at excitation and emission wavelengths of 544 and 590 nm, respectively.

Plasmids construction and siRNA transfection

Human FBXO2, FBXO6, and FBXO27 genes were amplified by polymerase chain reaction from total mRNA derived from HeLa cells pcDNA-6.2/N-EmGFP-DEST using Gateway technology (Invitrogen). Mutations, including FBXO2 ΔFBD, FBXO2 Y279A, FBXO2 W280A, and FBXO2 F279A/W280A, were generated by site-directed mutagenesis using a PrimeSTAR Mutagenesis Basal Kit (Takara). For knockdown experiments, cells were transfected with CUL1 siRNA oligonucleotides (D-004086; Dharmacon, Lafayette, CO, USA), SKP1 siRNA oligonucleotides (M-003323; Dharmacon), ROC1 siRNA oligonucleotides (CTM-583074; Dharmacon), FBXO2 siRNA (s25266, Thermo Fisher Scientific, Waltham, MA, USA), FBXO6 siRNA (s25337, Thermo Fisher Scientific), or non-targeting siRNAs (12935300, Thermo Fisher Scientific) using Lipofectamine 3000 (Invitrogen). Knockdown was confirmed by immunoblotting.

Antibodies and reagents

For Western blotting and immunofluorescence assays, the following antibodies were used: anti-FBXO2 (NBP2-55140; Novus Biologicals, Littleton, CO, USA), anti-FBXO2 (E-9; sc398111, Santa Cruz Biotechnology, Dallas, TX, USA, 1:1,000), anti-FBXO6 (NBP2-16451; Novus Biologicals), anti-SKP1 p19 (H-6; sc5281, Santa Cruz Biotechnology, 1:1,000), anti-CUL1 (D-5; sc17775, Santa Cruz Biotechnology, 1:1,000), anti-Rbx1/Roc1 (E-11; sc393640, Santa Cruz Biotechnology, 1:1,000), anti-p62 (H-290, Santa Cruz Biotechnology, 1:100), anti-FK2 (0918-2; Nippon Bio-Test Laboratories, Kyoto, Japan, 1:1,000), anti-LC3B (ab51520; Abcam, Cambridge, UK, 1:1,000), anti-LC3B (CTB-LC3-2-IC; Cosmo Bio, Japan, 1:100), anti-β-actin (D6A8; 8457; Cell Signaling Technology, Danvers, MA, USA, 1:1,000), anti-GAPDH (6C5; sc-32233; Santa Cruz Biotechnology, 1:1,000), and anti-GFP (GF200; 04363-24; Nacalai Tesque, 1:1,000). Horseradish peroxidase-conjugated anti-rabbit IgG (Jackson Laboratories, Bar Harbor, ME, USA), anti-mouse IgG (Jackson Laboratories), and anti-rabbit IgG (conformation-specific; L27A9; 5127; Cell Signaling Technology) were used as secondary antibodies for immunoblotting. Alexa Fluor 488-conjugated anti-mouse IgG (A32723; Invitrogen), Alexa Fluor 594-conjugated anti-mouse IgG (A32742; Invitrogen), and Alexa Fluor 594-conjugated anti-rabbit IgG (A32754; Invitrogen) were used as secondary antibodies for immunofluorescence. PYR41 (15226; 10 mM) and MLN4924 (15217; 0.3 µM) were purchased from Cayman Chemical (Ann Arbor, MI, USA).

Bacterial infection and viability assay

HeLa cells (5×10^4 cells/well) were cultured in 24-well culture plates and infected GAS strains at a multiplicity of infection (MOI) 100. After an appropriate incubation period, the cells were washed with PBS, treated with 100 µg/ml gentamicin in DMEM to kill extracellular bacteria, and lysed in sterile distilled water. Serial dilutions of the lysates were plated on THY agar plates. Colony counting was used to determine the number of invading and surviving GAS; the bacterial invasion data are presented as the ratio of "total intracellular GAS at 2 h" to "total adhesion GAS at 1 h", and the bacterial survival data are presented as the ratio of "intracellular live GAS at 6 h" to "total intracellular GAS at 2 h".

Generation of knockout cell lines using CRISPR/Cas9

CRISPR/Cas9 was used to knockout FBXO2. CRISPR guide (g)RNAs were designed to target an exon common to all splicing variants of the gene of interest (5'-ACCTTCTGCGTAACCCGTGTGGG-3'). HeLa cells were transfected with the vector hCAS9 (Addgene, Watertown, MA, USA, #41815) and gRNA-hyg vector containing the CRISPR target sequence. Untransfected cells were removed by selecting plates containing 300 µg/ml hygromycin B (Nacalai Tesque) and 750 µg/ml neomycin (G418; Nacalai Tesque). Single colonies were expanded, and depletion of the target gene was confirmed by immunoblotting. As a secondary screen for some KO cell lines, genomic DNA was isolated, and target regions were amplified by PCR and sequenced to confirm the presence of the desired frame-shift insertions and deletions.

Fluorescence microscopy

Cells were seeded onto 0.1% gelatin-coated coverslips in a 24-well plate at 5×10^4 cells/well, followed by infection with GAS at an MOI of 100. Cells were fixed for 15 min with 4% paraformaldehyde in PBS, washed with PBS, permeabilized with 0.1% Triton X-100 in PBS for 10 min, and blocked with 2% bovine serum albumin and 0.02% NaN₃ in PBS at room temperature for 1 h. The cells were then probed with primary antibody in blocking solution at 4°C overnight and labeled with secondary antibody at room temperature for 2 h. Cellular and bacterial DNAs were stained with DAPI. Confocal fluorescence micrographs were acquired using an FV1000 laser-scanning microscope (Olympus, Tokyo, Japan). To quantify the recruitment of marker (or proteins of interest) to intracellular bacteria, we counted the number of cells with a marker by eye using a confocal laser-scanning microscope (FV1000). We previously confirmed that the percentage of cells with LC3-positive bacteria and percentage of LC3-positive bacteria showed similar results (Toh et al, 2020).

In vitro GAS-FBXO2 binding assay

Logarithmic phase bacterial cultures (1 ml) were harvested, washed, and resuspended in PBS. Bacterial cells (WT and Δ gacI GAS) were mixed with HeLa cell lysate expressing EmGFP, EmGFP-FBXO2, or EmGFP-FBXP2 mutants. After incubation at 4°C for 2 h, the bacteria were extensively washed with PBS and then precipitated by centrifugation at 3,600 g at 4°C for 5 min. We repeated the washing step 4 times and measured fluorescence intensity with a multi-label plate reader Wallac 1420 ARVOsx (PerkinElmer).

Bacteria isolation from host cells

To isolate bacteria from infected host cells for biochemical analysis, HeLa cells were seeded into six-well plate and infected with GAS at an MOI 100. At 1 h after infection, the cells were washed with PBS and further incubated for 3 h in medium containing 100 µg/ml gentamicin (total 4-h infection). The cells were washed PBS and treated with distilled water to cause osmotic imbalance that disrupted the host plasma membrane and endosomal membranes. The lysates were reacted with anti-lipoteichoic acid antibody (MA1-40134, Thermo Fisher Scientific) for 2 h at 4°C and incubated with

Protein G-Magnetic Beads (MBL Life Science, Woburn, MA, USA) for 1 h. Immunoprecipitates were collected by a magnet and washed five times with PBS for analysis by immunoblotting. We determined the number of isolated bacteria by colony counting.

Immunoprecipitation

Cells expressing the indicated proteins were harvested, washed with PBS, and lysed for 30 min on ice in lysis buffer containing 10 mM Tris-HCl pH 7.4, 150 mM NaCl, 10 mM MgCl₂, 1 mM EDTA, 1% Triton X-100, and proteinase inhibitor cocktail (Nacalai Tesque). Lysates were then centrifuged, and the supernatants were pre-cleared for 30 min at 4°C with Protein G Sepharose Fast Flow (GE Healthcare Life Sciences, Little Chalfont, UK). After brief centrifugation, the supernatants were reacted for 2 h at 4°C with appropriate antibodies and incubated in Protein G Sepharose beads, with mixing, for another 1 h at 4°C. Immunoprecipitates were collected by brief centrifugation, washed five times with lysis buffer, and analyzed by immunoblotting.

Statistical analysis

Each protein-positive GAS was quantified by direct visualization using a confocal microscope. Unless otherwise indicated, values included in graphs represent the mean \pm standard error of the mean. Statistical analysis was performed by two-tailed Student's *t*-test at two groups and by pairwise *t*-test (*P*-value was adjusted by Bonferroni correction) for more than two groups. *P*-values < 0.05 were considered to indicate statistical significance and are marked with asterisks.

Data availability

This study includes no data deposited in external repositories.

Expanded View for this article is available online.

Acknowledgements

This work was supported in part by a Grant-in-Aid for Scientific Research (21K19376, 21K07023, 19H03471), by The Japan Agency for Medical Research and Development (AMED) (20fk0108073h0003, 20fk0108130h0401), by Takeda Science foundation (to T. N.), by The Chemo-Sero-Therapeutic Research Institute (to T. N.), and by Daiichi Sankyo Foundation of Life Science (to I. N.).

Author contributions

AY, TN, and IN conceived the study, provided reagents, and wrote the paper. AY, MH, and TN performed experiments and analyzed data.

Conflict of interest

The authors declare that they have no conflict of interest.

References

- Barnett T, Liebl D, Seymour L, Gillen C, Lim J, Larock C, Davies M, Schulz B, Nizet V, Teasdale, R, et al (2013) The globally disseminated M1T1 clone of Group A Streptococcus evades autophagy for intracellular replication. *Cell Host Microbe* 14: 675–682

- Boyle KB, Randow F (2013) The role of “eat-me” signals and autophagy cargo receptors in innate immunity. *Curr Opin Microbiol* 16: 339–348
- Campoy E, Colombo M (2006) Autophagy in intracellular bacterial infection. *Biochimica et Biophysica Acta* 1793: 1465–1477
- Chai Q, Wang X, Qiang L, Zhang Y, Ge P, Lu Z, Zhong Y, Li B, Wang J, Zhang L, et al (2019) A *Mycobacterium tuberculosis* surface protein recruits ubiquitin to trigger host xenophagy. *Nat Commun* 10: 1973
- Chauhan S, Kumar S, Jain A, Ponpuak M, Mudd M, Kimura T, Choi S, Peters R, Mandell M, Bruun J-A et al (2016) TRIMs and galectins globally cooperate and TRIM16 and galectin-3 co-direct autophagy in endomembrane damage homeostasis. *Dev Cell* 39: 13–27
- Cole JN, Barnett TC, Nizet V, Walker MJ (2011) Molecular insight into invasive group A streptococcal disease. *Nat Rev Microbiol* 9: 724–736
- Franco LH, Nair VR, Scharn CR, Xavier RJ, Torrealba JR, Shiloh MU, Levine B (2017) The ubiquitin ligase Smurf1 functions in selective autophagy of *Mycobacterium tuberculosis* and anti-tuberculous host defense. *Cell Host Microbe* 21: 59–72
- Fujita N, Morita E, Itoh T, Tanaka A, Nakaoka M, Osada Y, Umemoto T, Saitoh T, Nakatogawa H, Kobayashi S, et al (2013) Recruitment of the autophagic machinery to endosomes during infection is mediated by ubiquitin. *J Cell Biol* 203: 115–128
- Glenn KA, Nelson RF, Wen HM, Mallinger AJ, Paulson HL (2008) Diversity in tissue expression, substrate binding, and SCF complex formation for a lectin family of ubiquitin ligases. *J Biol Chem* 283: 12717–12729
- Henningham A, Davies MR, Uchiyama S, van Sorge NM, Lund S, Chen KT, Walker MJ, Cole JN, Nizet V (2018) Virulence role of the GlcNAc side chain of the lancefield cell wall carbohydrate antigen in non-M1-serotype group A *Streptococcus*. *MBio* 9: e02294-17
- Huett A, Heath RJ, Begun J, Sassi SO, Baxt LA, Vyas JM, Goldberg MB, Xavier RJ (2012) The LRR and RING domain protein LRSAM1 is an E3 ligase crucial for ubiquitin-dependent autophagy of intracellular *Salmonella* Typhimurium. *Cell Host Microbe* 12: 778–790
- Ito C, Saito Y, Nozawa T, Fujii S, Sawa T, Inoue H, Matsunaga T, Khan S, Akashi S, Hashimoto R et al (2013) Endogenous nitrated nucleotide is a key mediator of autophagy and innate defense against bacteria. *Mol Cell* 52: 794–804
- Levine B, Deretic V (2007) Unveiling the roles of autophagy in innate and adaptive immunity. *Nat Rev Immunol* 7: 767–777
- Lin CY, Nozawa T, Minowa-Nozawa A, Toh H, Aikawa C, Nakagawa I (2019) LAMTOR2/LAMTOR1 complex is required for TAX1BP1-mediated xenophagy. *Cell Microbiol* 21: e12981
- Liu EA, Schultz ML, Mochida C, Chung C, Paulson HL, Lieberman AP (2020) Fbxo2 mediates clearance of damaged lysosomes and modifies neurodegeneration in the Niemann-Pick C brain. *JCI Insight* 5: e136676
- Lu SL, Kawabata T, Cheng YL, Omori H, Hamasaki M, Kusaba T, Iwamoto R, Arimoto H, Noda T, Lin YS et al (2017) Endothelial cells are intrinsically defective in xenophagy of *Streptococcus pyogenes*. *PLoS Pathog* 13: e1006444
- Manzanillo PS, Ayres JS, Watson RO, Collins AC, Souza G, Rae CS, Schneider DS, Nakamura K, Shiloh MU, Cox JS (2013) The ubiquitin ligase parkin mediates resistance to intracellular pathogens. *Nature* 501: 512–516
- McCarty M (1952) The lysis of group A hemolytic streptococci by extracellular enzymes of *Streptomyces albus*. II. Nature of the cellular substrate attacked by the lytic enzymes. *J Exp Med* 96: 569–580
- Minowa-Nozawa A, Nozawa T, Okamoto-Furuta K, Kohda H, Nakagawa I (2017) Rab35 GTPase recruits NDP52 to autophagy targets. *EMBO J* 36: 2790–2807
- Mizushima T, Hirao T, Yoshida Y, Lee SJ, Chiba T, Iwai K, Yamaguchi Y, Kato K, Tsukihara T, Tanaka K (2004) Structural basis of sugar-recognizing ubiquitin ligase. *Nat Struct Mol Biol* 11: 365–370
- Nakagawa I, Amano A, Mizushima N, Yamamoto A, Yamaguchi H, Kamimoto T, Nara A, Funao J, Nakata M, Tsuda K, et al (2004) Autophagy defends cells against invading group A *Streptococcus*. *Science* 306: 1037–1040
- Nagata Y, Burger MM (1974) Wheat germ agglutinin. Molecular characteristics and specificity for sugar binding. *J Biol Chem* 249: 3116–3122
- Noad J, von der Malsburg A, Pathe C, Michel MA, Komander D, Randow F (2017) LUBAC-synthesized linear ubiquitin chains restrict cytosol-invading bacteria by activating autophagy and NF- κ B. *Nat Microbiol* 2: 17063
- Nozawa T, Sano S, Minowa-Nozawa A, Toh H, Nakajima S, Murase K, Aikawa C, Nakagawa I (2020) TBC1D9 regulates TBK1 activation through Ca(2+) signaling in selective autophagy. *Nat Commun* 11: 770
- Ogawa M, Matsuda R, Takada N, Tomokiyo M, Yamamoto S, Shizukushi S, Yamaji T, Yoshikawa Y, Yoshida M, Tanida I et al (2018) Molecular mechanisms of *Streptococcus pneumoniae*-targeted autophagy via pneumolysin, Golgi-resident Rab41, and Nedd4-1-mediated K63-linked ubiquitination. *Cell Microbiol* 20: e12846
- O’Seaghdha M, Wessels M (2019) Streptolysin O and its co-toxin NAD-glycohydrolase protect group A *Streptococcus* from Xenophagic killing. *PLoS Pathog* 9: e1003394
- Otten EG, Werner E, Crespillo-Casado A, Boyle KB, Dharamdasani V, Pathe C, Santhanam B, Randow F (2021) Ubiquitylation of lipopolysaccharide by RNF213 during bacterial infection. *Nature* 594: 111–116
- Paz I, Sachse M, Dupont N, Mounier J, Cederfur C, Enninga J, Leffler H, Poirier F, Prevost M-C, Lafont F et al (2010) Galectin-3, a marker for vacuole lysis by invasive pathogens. *Cell Microbiol* 12: 530–544
- Rush JS, Edgar RJ, Deng P, Chen J, Zhu H, van Sorge NM, Morris AJ, Korotkov KV, Korotkova N (2017) The molecular mechanism of N-acetylglucosamine side-chain attachment to the Lancefield group A carbohydrate in *Streptococcus pyogenes*. *J Biol Chem* 292: 19441–19457
- Thurston TL, Wandel MP, von Muhlinen N, Foeglein A, Randow F (2012) Galectin 8 targets damaged vesicles for autophagy to defend cells against bacterial invasion. *Nature* 482: 414–418
- Toh H, Nozawa T, Minowa-Nozawa A, Hikichi M, Nakajima S, Aikawa C, Nakagawa I (2020) Group A *Streptococcus* modulates RAB1- and PIK3C3 complex-dependent autophagy. *Autophagy* 16: 334–346
- van Sorge N, Cole J, Kuipers K, Henningham A, Aziz R, Kasirer-Friede A, Lin L, Berends E, Davies M, Dougan G et al (2014) The classical lancefield antigen of group a *Streptococcus* is a virulence determinant with implications for vaccine design. *Cell Host Microbe* 15: 729–740
- Xu Y, Zhou P, Cheng S, Lu Q, Nowak K, Hopp A-K, Li L, Shi X, Zhou Z, Gao W et al (2019) A bacterial effector reveals the V-ATPase-ATG16L1 axis that initiates Xenophagy. *Cell* 178: 552–566.e20
- Yang Y, Kitagaki J, Dai R-M, Tsai YC, Lorick KL, Ludwig RL, Pierre SA, Jensen JP, Davydov IV, Oberoi P et al (2007) Inhibitors of ubiquitin-activating enzyme (E1), a new class of potential cancer therapeutics. *Can Res* 67: 9472–9481
- Yoshida Y, Chiba T, Tokunaga F, Kawasaki H, Iwai K, Suzuki T, Ito Y, Matsuoka K, Yoshida M, Tanaka K et al (2002) E3 ubiquitin ligase that recognizes sugar chains. *Nature* 418: 438–442
- Yoshida Y, Yasuda S, Fujita T, Hamasaki M, Murakami A, Kawawaki J, Iwai K, Saeki Y, Yoshimori T, Matsuda N et al (2017) Ubiquitination of exposed glycoproteins by SCF(FBXO27) directs damaged lysosomes for autophagy. *Proc Natl Acad Sci USA* 114: 8574–8579
- Zhou X, Zhao G, Truglio JJ, Wang L, Li G, Lennarz WJ, Schindelin H (2006) Structural and biochemical studies of the C-terminal domain of mouse peptide-N-glycanase identify it as a mannose-binding module. *Proc Natl Acad Sci USA* 103: 17214–17219